Simultaneous Observations of Cirrus Clouds with a Millimeter-Wave Radar and the MU Radar

EIKO WADA, HIROYUKI HASHIGUCHI, MASAYUKI K. YAMAMOTO, MICHIHIRO TESHIBA, AND SHOICHIRO FUKAO

Research Institute for Sustainable Humanosphere, Kyoto University, Uji, Kyoto, Japan

(Manuscript received 20 August 2003, in final form 25 July 2004)

ABSTRACT

Observations of frontal cirrus clouds were conducted with the scanning millimeter-wave radar at the Shigaraki Middle and Upper Atmosphere (MU) Radar Observatory in Shiga, Japan, during 30 September–13 October 2000. The three-dimensional background winds were also observed with the very high frequency (VHF) band MU radar. Comparing the observational results of the two radars, it was found that the cirrus clouds appeared coincident with the layers of the strong vertical shear of the horizontal winds, and they developed and became thicker under the condition of the strong vertical shear of the horizontal wind and updraft. The result of the radiosonde observation indicated that Kelvin–Helmholtz instability (KHI) occurred at 8–9-km altitudes because of the strong vertical shear of the horizontal wind. The warm and moist air existed above the 8.5-km altitude, and the cold and dry air existed below the 8.5-km altitude. As a result of the airmass mixing of air above and below the 8.5-km altitudes, the cirrus clouds were formed. The updraft, which existed at 8.5–12-km altitude, caused the development of the cirrus clouds with the thickness of >2 km. By using the scanning millimeter-wave radar, the three-dimensional structure of cell echoes formed by KHI for the first time were successfully observed.

1. Introduction

A cirrus cloud, which is formed in the upper troposphere, consists of ice crystals. It covers a relatively wide area and persists for a long time, so it affects the earth's radiation balance and may play an important role in the earth's climate. Moreover, ice crystals falling from cirrus clouds can be important seeding material for supercooled clouds in the middle troposphere (Braham 1967). However, observations of cirrus clouds with conventional meteorological radars with relatively long wavelengths (~6 cm) are difficult, because they occur at high altitudes and are composed of small ice crystals with various shapes and sizes. Therefore, their detailed microphysical and dynamical structures and radiative characteristics had been uncertain for a long time. Recently, new remote sensing techniques and in situ measurements permit observations of various dynamical and physical properties of cirrus clouds. For example, in June 1989 the Meteorological Research Institute (MRI) carried out ground-based observations of cirrus clouds using a lidar, various radiometers, and the hydrometeor-videosonde (HYVIS; e.g., Uchiyama et al. 1999; Uchiyama and Fukabori 1999). Further, airborne in situ observations have provided information on cirrus cloud particle size distributions and ice crystal shapes (e.g., Arnott et al. 1995; Gayet et al. 1996; Heymsfield and McFarquhar 1996).

A millimeter-wave radar has enough sensitivity to observe small crystals because of its short wavelength (~8 mm). Therefore, it is one of the most effective remote sensing instruments for cirrus cloud observation. In the First International Satellite Cloud Climatology Project (ISCCP) Regional Experiment (FIRE) II in Kansas in 1991 (e.g., Gultepe et al. 1995; Stephens 1995) and in the European Cloud and Radiation Experiment 1994 (EUCREX'94) off of the coast of Brittany (France) over the Atlantic Ocean (e.g., Sauvage et al. 1999; Chepfer et al. 1999), and in the U.S. Department of Energy (DOE) Atmospheric Radiation Measurement (ARM) Program (Stokes and Schwartz 1994), simultaneous observations of cirrus clouds were conducted using millimeter-wave radar and aircraft. The ARM radars have been continuously operating in Oklahoma and Alaska, in addition to three locations in the Pacific Ocean area. Since 1994, extensive cirrus cloud observation have been conducted on a roughly biennial basis at the Southern Great Plains ARM site in Oklahoma (Lynch et al. 2002). However, most of these millimeter-wave radars had fixed vertical-pointing an-

Corresponding author address: Dr. Eiko Wada, Research Institute for Sustainable Humanosphere, Kyoto University, Gokasho, Uji, Kyoto 611-0011, Japan.
E-mail: wada@rish.kyoto-u.ac.jp

tennas. Further, aircraft could not continuously observe the area where millimeter-wave radars observe.

Simultaneous observations of the spatial structure of cirrus clouds and the three-dimensional motion of the background atmosphere make it possible to study the structure and properties of cirrus clouds in more detail. However, the simultaneous observation of cirrus clouds and background atmospheric motion, including vertical velocity, have been hardly conducted, because observations with a wind profiler are necessary to continuously observe the background atmospheric condition in and around cirrus clouds.

We carried out simultaneous observations of cirrus clouds using the millimeter-wave Doppler radar (hereinafter referred to as the mm-wave radar) and the Middle and Upper Atmosphere (MU) radar. The MU radar is a wind profiler operated at a very high frequency (VHF). It is installed at the Shigaraki MU Observatory in Shigaraki, Shiga, Japan (34.85°N, 136.10°E; Fukao et al. 1985a,b). The mm-wave radar used in this study has a steerable antenna. Therefore, we could observe the three-dimensional structure of the cirrus clouds. The instruments used in this study are described in section 2, the observations are presented in section 3, and the summary is given in section 4.

2. Observations

The mm-wave radar has good transportability because all of the equipment is mounted on a truck. We transported it to the Shigaraki MU Observatory and conducted a simultaneous observation with the mm-wave radar and the MU radar during 30 September–13 October 2000. The cirrus clouds appeared for the four days of 3, 5, 6, and 7 October. Observation results on 5 and 6 October will be discussed in the following sections. We used the mm-wave radar and the MU radar to observe the inner structure of cirrus clouds and background winds, respectively. We launched a radiosonde from the MU Observatory at 1500 LT on 6 October to obtain vertical profiles of atmospheric temperature and humidity.

a. The mm-wave Doppler radar

Mitsubishi Electric Corporation and Research Institute for Sustainable Humanosphere [(RISH), formerly the Radio Science Center for Space and Atmosphere (RASC)] of Kyoto University have collaboratively developed the mm-wave radar (Hamazu et al. 2000, 2003). Table 1 shows the principal specifications of the mm-wave radar. The operational frequency is 34.75 GHz (Ka band), and the peak transmitting power is 100 kW. Because of a short operating wavelength (8.6 mm) and high transmitting power, this radar has a good sensitivity for cloud and fog particles (Hamazu et al. 2000, 2001). The highest range resolution of the mm-wave radar is 62.5 m if it obtains only reflectivity data. However, because of the limitation of the throughput of the signal-processing computer, the radar can obtain both reflectivity and Doppler velocity simultaneously only with the range resolution of 125 m. Therefore, the range resolution used in this observation was limited to 125 m. The antenna is a 2-m-diameter parabolic antenna of the Cassegrain type and is capable of scanning 360° in azimuth, from −2° to +92° in elevation at 6 rpm maximum. We used a rotation speed of 1 rpm for this observation. The mm-wave radar can be operated with the antenna with seven scanning modes such as plan position indicator (PPI), range–height indicator (RHI), constant altitude PPI (CAPPI), sector, sector PPI (SPPI), sector RHI (SRHI), and position (POS). SRHI and CAPPI modes are mainly used in the observation.

TABLE 1. Principal specifications of the mm-wave Doppler radar.

Operational frequency	34.75 GHz (Ka band)
Antenna type	Cassegrain (2-m diameter)
Antenna gain	54 dB*i*
Beamwidth	0.3°
Transmitter type	Magnetron
Peak transmitting power	100 kW
Duty ratio	0.05% (max)
Interpulse period (IPP)	450, 4500 Hz (pulse pair)
Data digitization	12 bits
Range data sampling	2.4 MHz (62.5 m) for non-Doppler observation, 1.2 MHz (125 m) for Doppler observation
Resolution of Doppler velocity	0.1 m s^{-1}
Sensitivity	−27 dB*Z* at 10-km range, −16 dB*Z* at 20-km range
Transmitting pulse width	0.5 μs
Polarization	Horizontal
Horizontal rotation	6 rpm (max)

b. The MU radar

The MU radar is one of the largest atmospheric radars in the world. The MU radar is a 46.5-MHz monostatic Doppler radar with an active phased-array antenna with a 103 m diameter, composed of 475 Yagi antennas and with 1-MW peak output power. The MU radar can steer the total antenna beam to any direction up to a zenith angle of 30°. The MU radar can observe air velocity information in any weather condition because it receives scattering echoes from fluctuations of the radar refractive index in the clear air. We can obtain altitude profiles of a wind vector including a vertical velocity and echo power intensities in the troposphere and the lower stratosphere with fine time and height resolutions of 3 min and 150 m, respectively. The accuracy of one profile of vertical wind is about 0.2 m s^{-1} (Yamamoto et al. 1988). In this paper, we averaged two profiles by computing vertical profiles of winds. Therefore, the accuracy of vertical wind improves up to $0.2/\sqrt{2} = 0.14$ m s^{-1}. Even in precipitating conditions, the MU radar can observe three components of air velocity

and the falling speed of precipitating particles simultaneously (e.g., Wakasugi et al. 1986; Sato et al. 1990). Therefore, we can examine the motion of background wind in cirrus cloud conditions.

3. Observation results

a. Synoptic weather situation on 5 and 6 October 2000

Figure 1 shows the dewpoint depression and the horizontal wind derived from regional objective analysis (RANAL) data at 300 hPa at 0900 LT (0000 UTC) 5 and 6 October 2000. The time resolution of RANAL data is 2 times per day [0000 (0900) and 1200 UTC (2100 LT)]. To examine if the relative humidity data derived from RANAL matched the result of the radiosonde observation, we estimated the relative humidity at the 350-hPa level (8-km altitude at which the cirrus clouds existed) at 0600 UTC (1500 LT) 6 October by interpolating data at 0000 and 1200 UTC 6 October and compared it with one derived from the radiosonde observation. The relative humidity was derived from 66% at 350 hPa. On the other hand, the relative humidity measured by the radiosonde at 1500 LT was 69% at the equivalent level. Therefore, the relative humidity derived from RANAL data agrees well with the result by the radiosonde. Figure 2 shows the infrared (IR) blackbody brightness temperature (T_{BB}) from the Geostationary Meteorological Satellite (GMS) at 1300 LT (0400 UTC) 5 October and at 1400 LT (0500 UTC) 6 October 2000. A front existed in the south of the Japanese islands on 5 October and moved northward. A jet core parallel to the front line was located to the north of

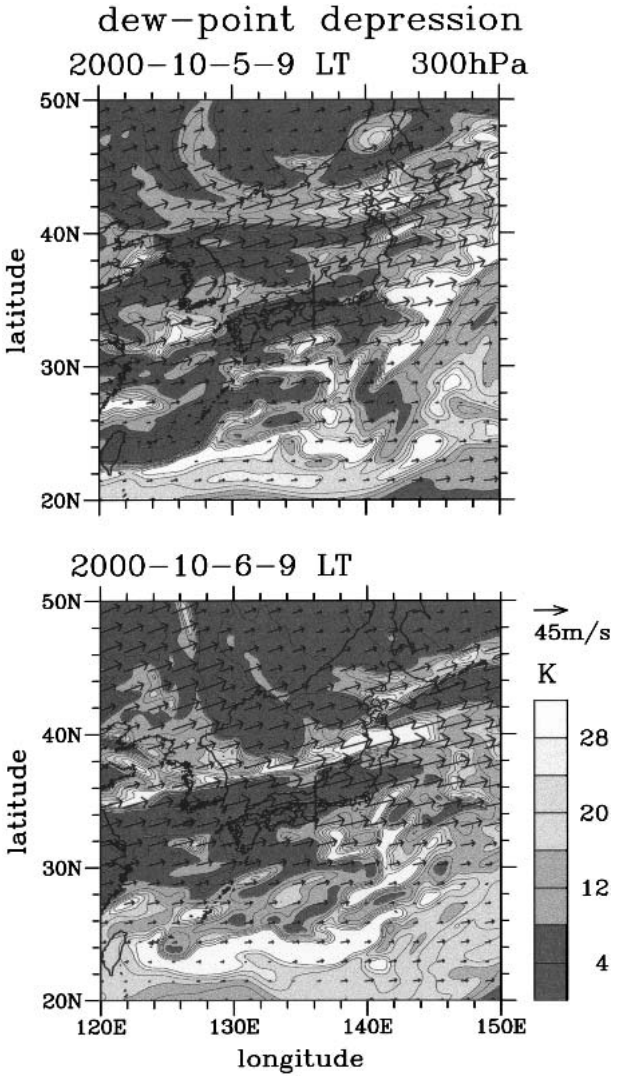

FIG. 1. Horizontal distribution of dewpoint depression (contour) and horizontal wind (arrows) of RANAL data at 300 hPa at 0000 UTC (0900 LT) (top) 5 and (bottom) 6 Oct 2000. Plus signs (+) indicate the location of the MU Observatory.

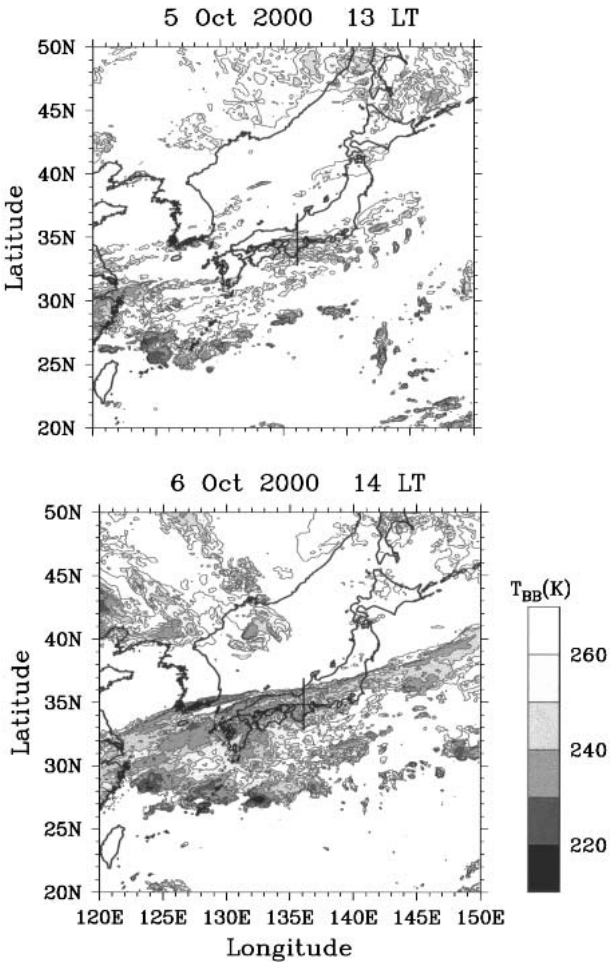

FIG. 2. Horizontal distribution of T_{BB} of GMS data at (top) 0400 UTC (1300 LT) 5 Oct and (bottom) 0500 UTC (1400 LT) 6 Oct 2000. Plus signs (+) indicate the location of the MU Observatory.

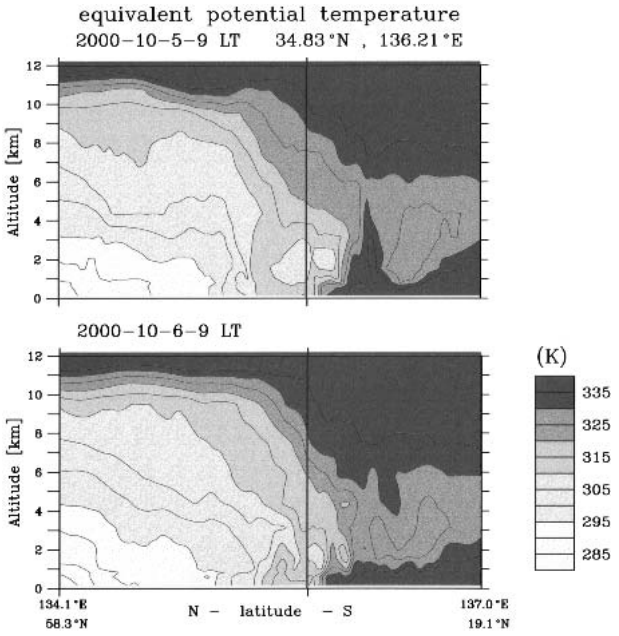

FIG. 3. Latitude–altitude variations of equivalent potential temperature of RANAL data at 0000 UTC (0900 LT) (top) 5 and (bottom) 6 Oct 2000. Vertical lines indicate the location of the MU Observatory.

the front (33°N, 135°E), and its maximum wind speed was more than 50 m s^{-1} (see Fig. 1). The cloud band with T_{BB} of <250 K extended from the front to the Kii peninsula and was located in the south of the jet stream on 5 October. The cloud band moved northward with the northward shift of the front line. On 6 October the cloud band extended from the front to the Japanese islands and covered the area from Kyushu to the Kanto plain, including the observation site. Low T_{BB} (<240 K), which is a typical characteristic of high-level cirrus clouds, was seen over the observation site. Figure 3 shows the latitude–altitude plots of the equivalent potential temperature derived from RANAL data at 0900 LT (0000 UTC) 5 October and at 0900 LT (0000 UTC) 6 October. The positive meridional gradient of the equivalent potential temperature is steeper at 7–10-km altitudes in the case on 6 October than the case on 5 October at the observation site. Larger updraft is expected at 7–10-km altitudes on 6 October and in fact it was observed by the MU radar (later shown in Figs. 7 and 11).

b. *The case of 5 October 2000*

1) SPATIAL STRUCTURE OF CIRRUS CLOUDS

Figure 4 shows time variations of the vertical cross section of reflectivity obtained with the SRHI mode of the mm-wave radar between 1404 and 1455 LT. We alternately observed in the two directions of 240° and 330° in azimuth. The antenna scanning time to obtain one azimuthal direction is about 15 s.

The directions of wind (70°–90°) and the vertical shear of the horizontal wind (45°–90°) were almost the same at 8–8.5-km altitudes, where the vertical shear was strong (>16 m s^{-1} km^{-1}, see Fig. 5c). Therefore, the direction of 240° (330°) at which the mm-wave radar

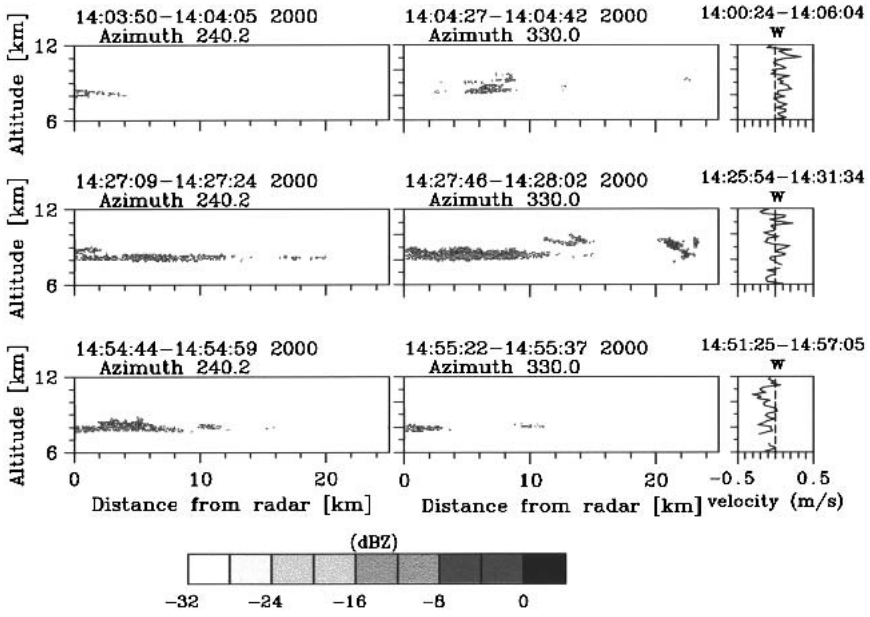

FIG. 4. RHI plots showing time variations of echo power observed with (left), (middle) the mm-wave radar and (right) height profiles of vertical velocity observed with the MU radar between 1400 and 1500 LT 5 Oct 2000. Azimuth angles are (left) 240° and (middle) 330°.

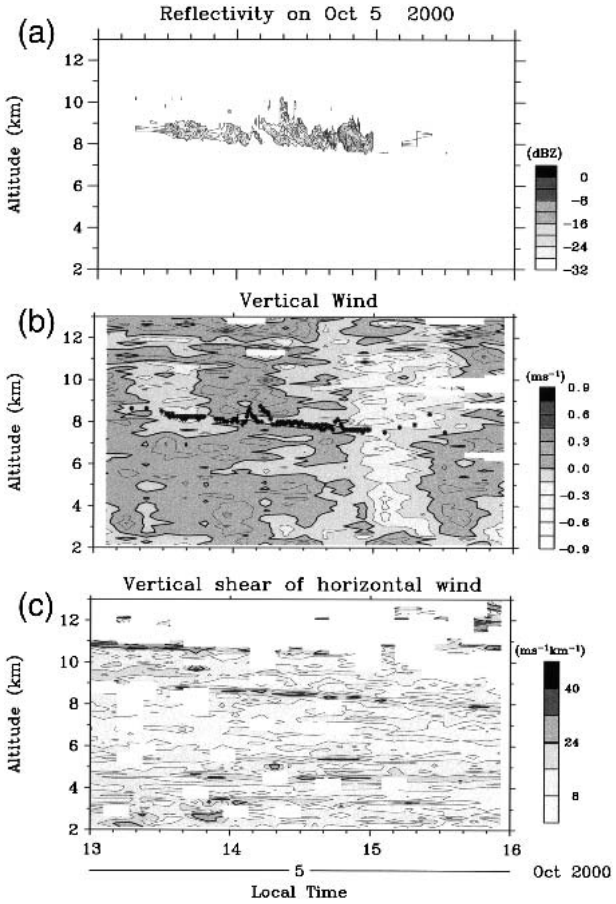

FIG. 5. Time–altitude variations of (a) echo power observed with the mm-wave radar, and (b) vertical velocity and (c) the vertical shear of the horizontal wind observed with the MU radar during 1300–1600 LT 5 Oct 2000. Asterisk symbols (*) indicate the altitudes of cloud bases observed with the mm-wave radar over the MU radar site.

observed with the SRHI mode was almost parallel (perpendicular) to both the directions of the horizontal wind and the vertical shear of the horizontal wind. The sensitivity of the mm-wave radar is limited to about -27 dBZ at the 10-km range, and about -16 dBZ at the 20-km range, respectively. Therefore, the mm-wave radar might fail to detect part of the cirrus clouds, especially in regions far from the radar.

At 1404 LT (Fig. 4, top panels), patchy weak echoes (clouds) appeared at an approximately 8-km altitude in both azimuthal directions. At 1427 LT, the stratiform echoes horizontally spread out at the same altitude in both azimuthal directions. At 1455 LT, the echoes from both directions were patchy and thin. Though the thickness of the cirrus clouds in the direction of 330° was slightly thicker than that in the direction of 270°, there was no significant difference in the structure of the cirrus clouds between the direction of 270° and 330°. The cirrus clouds disappeared completely after 1530 LT 5 October. As we mentioned above, there was no significant difference in the structure of the cirrus clouds between the directions that were parallel and perpendicular to the horizontal wind and the vertical shear of the horizontal wind. On the other hand, on 6 October the structure of the cirrus clouds in these two directions were different [later discussed in section 3c(1)].

2) VERTICAL WIND AND VERTICAL SHEAR OF HORIZONTAL WINDS OBSERVED BY THE MU RADAR

Figures 5a and 5b show time–altitude variations of reflectivity observed with the mm-wave radar and vertical wind obtained with the MU radar between 1300 and 1600 LT 5 October. These variations of vertical winds are reliable enough, because their accuracy is about 0.14 m s^{-1} (see section 2b).

We estimated the contamination effect of the horizontal wind on the vertical wind observed in the vertically pointing beam. The contamination occurs when Kelvin–Helmholtz instability (KHI) makes a slightly tilted echo layer observed by the vertically pointing beam. According to the equation of Muschinski (1996), the bias of the vertical wind by the horizontal wind is estimated as

$$\Delta w = -\frac{1}{2\pi \ln 2} \ln\left(\frac{P_m}{P_i}\right) \theta_{3\mathrm{dB}}{}^2 u \,\mathrm{sign}\left(\frac{\partial u}{\partial z}\right) \qquad (1)$$

(using the following notation: the bias of vertical wind Δw, the echo power observed when the beam is pointed perpendicularly to the refractivity surface P_m, the isotropic echo power P_i, one-way half-power beamwidth $\theta_{3\mathrm{dB}}$, the mean horizontal wind velocity u, and altitude z). When we apply Eq. (1), the maximum downward bias of the vertical wind was 0.05 m s^{-1} [$\theta_{3\mathrm{dB}} = 3.6°$, $P_m/P_i = 7$ dB, $u = 30$ m s^{-1}, sign$(\partial u/\partial z) = 1$] during 1420–1440 LT at the 8.4-km altitude. However, the contamination effect of the horizontal wind on the vertical wind measurement under the condition of KHI occurrence was very sporadic, when we consider that the background Brunt–Väisälä frequency squared (N^2) was 0.13×10^{-3} rad^2 s^{-2} (averaged value during the 8–10.5-km altitudes observed by the radiosonde), and that KHI could occur under the condition of $\partial u/\partial z > 23$ m s^{-1} km^{-1} (see Fig. 12, below). On 5 October the vertical shear of the horizontal wind was almost always weak (<23 m s^{-1} km^{-1}) even at 7.5–8.5-km altitudes (see Fig. 5c). Therefore, we consider that the contamination effect of the horizontal wind on the vertical wind measurement under the condition of KHI occurrence is almost negligible for the case of 5 October.

The MU radar observed the small area with a radius of 0.17 km at an 8-km altitude aloft, because the two-way half-power beamwidth of the MU radar is 2.5°. Nevertheless, the cirrus clouds passed over the MU radar on 5 October, and the MU radar could successfully

observe the background vertical wind in the cirrus clouds. At 1320–1340 and 1340–1440 LT, a weak updraft (up to 0.3 m s^{-1}) was dominant at the 2–7- and 3–12-km altitudes, respectively. At 1320–1340 LT there was a weak downdraft (approximately 0.3 m s^{-1}) at 7–11-km altitudes. Because cirrus clouds cannot be developed in the downdraft, it is considered that we observed decaying cirrus clouds advected from the east during 1320–1340 LT. During 1440–1500 LT, the vertical wind became a weak downdraft (approximately 0–0.45 m s^{-1}) at 2–12-km altitudes. With the occurrence of the downdraft, the cirrus clouds disappeared. It suggests that ice crystals in the cirrus clouds moved downward due to this downdraft, sublimed, and then disappeared.

Time–altitude variations of the vertical shear of the horizontal wind observed with the MU radar are shown in Fig. 5c. At 7.5–8.5-km altitudes, the strong shear layer existed and descended with time during 1330–1600 LT. During 1330–1500 LT, the vertical shear was strong (>16 m s^{-1} km^{-1}) above the cirrus cloud base (7.5–8.5-km altitudes). During 1420–1440 LT, the vertical shear was significantly strong (24–40 m s^{-1} km^{-1}). At 1428 LT a slightly more intense and thicker echo (up to a 10-km altitude) appeared over the MU Observatory (see Fig. 4). On 6 October the result of the radiosonde observation strongly suggested that KHI occurred where the vertical shear of the horizontal wind exceeded 23 m s^{-1} km^{-1}. It suggests that KHI occurred around 1420–1440 LT on 5 October because the vertical shear of the horizontal wind exceeded the threshold of 23 m s^{-1} km^{-1} (>24 m s^{-1} km^{-1}), and that KHI might play some role on the formation of cirrus clouds with large particles. Fortunately, the cirrus clouds passed over the MU radar also on 6 October when the vertical shear of the horizontal wind at 8–9-km altitudes was stronger than the shear on 5 October. The role of KHI on the formation of cirrus clouds will be discussed in detail in section 3c.

3) Vertical Doppler velocity observed by the millimeter-wave radar

Figure 6 shows time–altitude variations of vertical Doppler velocity observed with the mm-wave radar during 1300–1600 LT 5 October, and Fig. 7 shows the averaged profiles of the vertical wind observed with the MU radar and the vertical Doppler velocity observed with the mm-wave radar during 1400–1500 LT 5 October.

The vertical wind observed with the MU radar was about 0 m s^{-1} at a 7.5–10-km altitude (Fig. 7). Therefore, we can regard the vertical Doppler velocity observed with the mm-wave radar as the reflectivity-weighted particle fall velocity. It might cause insufficient development of the cirrus clouds with large particles (see Fig. 5a).

The reflectivity-weighted particle fall velocity inside the cirrus clouds was between 2 and 1 m s^{-1}. It shows

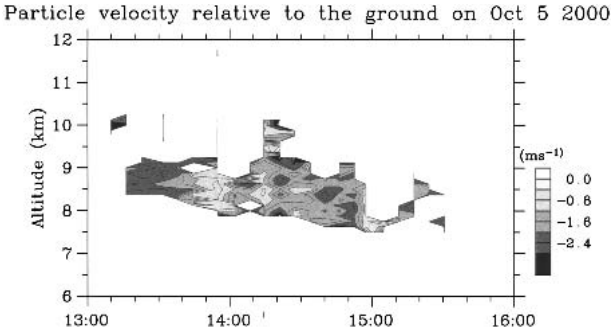

FIG. 6. Time–altitude variations of vertical Doppler velocity observed with the mm-wave radar during 1300–1600 LT 5 Oct 2000.

that the mm-wave radar has sufficient sensitivity for a large particle whose fall velocity is larger than 1 m s^{-1}. Though the cirrus clouds with small particles might exist above a 10-km altitude, we can conclude that the cirrus clouds with large particles did not develop well in the absence of sufficient updraft.

c. *The case of 6 October 2000*

1) Spatial structure of clouds

Figure 8 shows time variations of reflectivity obtained with the SRHI mode of the mm-wave radar in

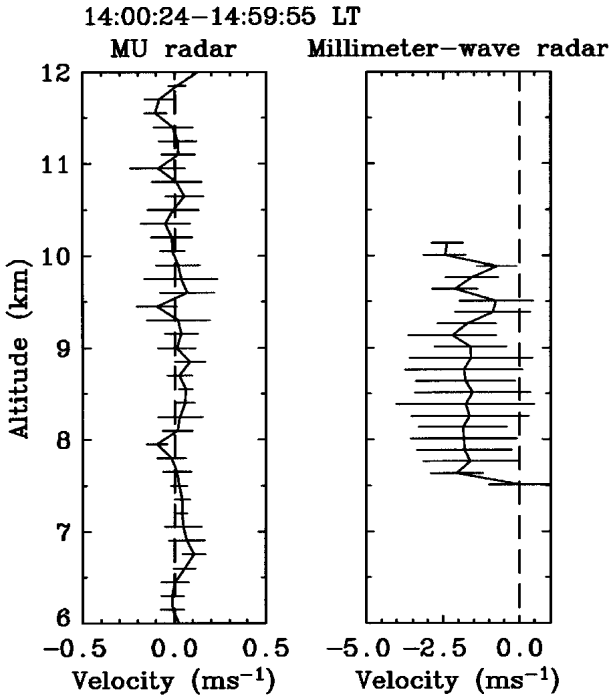

FIG. 7. Altitude profiles of the vertical wind observed with the MU radar and vertical Doppler velocity observed with the mm-wave radar averaged during 1400–1500 LT 5 Oct 2000. The horizontal lines indicate a standard deviation.

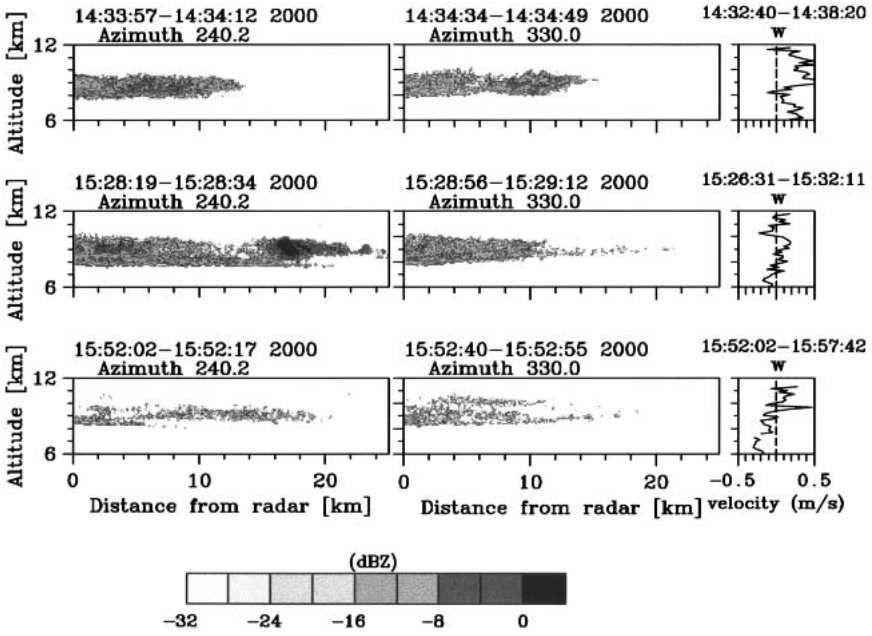

FIG. 8. Same as Fig. 4, but for 1430–1600 LT 6 Oct 2000.

the two directions of 240° and 330° in azimuth for 1434–1552 LT on 6 October. The directions of wind (70°–90°) and the vertical shear of the horizontal wind (45°–90°) were almost the same at 8–9-km altitudes where the vertical shear was strong (>16 m s^{-1} km^{-1}). These conditions were not changed between 5 and 6 October.

At 1434 LT, stratiform echoes appeared at 7.5–9.5-km altitudes in both azimuthal directions, and spread horizontally at a 0–15-km distance from the mm-wave radar. At 1528 LT, the stratiform echoes in both directions existed at the same altitude as those at 1434 LT. However, the cirrus clouds in the 240° direction contained strong echo cells at approximately a 17-km distance from the radar. These cell echoes will be discussed in detail in section 3c(5). At 1552 LT, the stratiform echoes became very weak. The cloud-base height was higher (8.5-km altitude) than that at 1434 LT (8-km altitude). During 1434–1552 LT the cirrus clouds were thick and unevenly distributed in the direction parallel to the horizontal wind and the vertical shear of the horizontal wind (240°). On the other hand, the cirrus clouds were thick and had the relatively uniform distribution in the direction perpendicular to the direction of the horizontal wind and the vertical shear of the horizontal wind (330°). It shows that a different spatial distribution of cirrus clouds existed in the direction of 240° and 330° on 6 October. Further, the cirrus clouds with large particles were thicker on 6 than on 5 October (see Figs. 4 and 8). Hereinafter, we will discuss the reason why a different distribution of the cirrus clouds existed in the direction of 240° and 330°, and why thick cirrus clouds with large particles developed on 6 October.

2) VERTICAL WIND AND VERTICAL SHEAR OF HORIZONTAL WIND OBSERVED BY THE MU RADAR

Figures 9a and 9b show time–altitude variations of reflectivity observed with the mm-wave radar and the vertical wind obtained with the MU radar during 1400–1700 LT. We estimated the contamination effect of the horizontal wind on the vertical wind observed by the vertically pointing beam with Eq. (1). The maximum downward bias of vertical wind was 0.08 m s^{-1} [P_m/P_i = 8 dB, u = 45 m s^{-1}, sign($\partial u/\partial z$) = 1] at the 8.8-km altitude during 1420–1430 LT. KHI might occur during this period, because the vertical shear of the horizontal wind was strong enough (>40 m s^{-1} km^{-1}) to generate KHI, when we used N^2 of 0.13×10^{-3} rad^2 s^{-2}. However, the averaged downward bias of the vertical wind was only 0.03 m s^{-1} [P_m/P_i = 3.6 dB, u = 33 m s^{-1}, sign($\partial u/\partial z$) = 1] at 8–9-km altitudes during 1400–1700 LT, when and where KHI occurred. Further, the contamination effect of the horizontal wind on the vertical wind measurement did not exist except at 8–9 km altitudes, because the vertical shear of the horizontal wind was weak (<23 m s^{-1} km^{-1}) everywhere, except for this altitude. Therefore, our finding that an updraft of 0–0.3 m s^{-1} existed in the cirrus clouds is a reliable result.

During 1430–1550 LT, an updraft was dominant at 8–12-km altitudes, and the maximum updraft (>0.75 m s^{-1}) was stronger than that on 5 October (up to 0.3 m s^{-1}). However, the downdraft region below 8 km extended with time after 1430 LT. Around 1430 and 1520

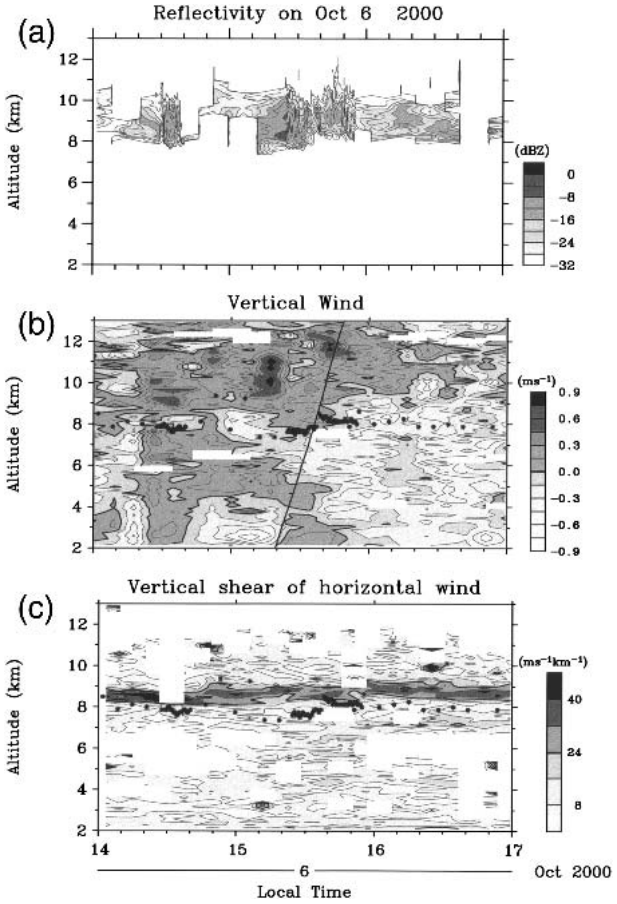

FIG. 9. Same as Fig. 5, but for 1400–1700 LT 6 Oct 2000. Asterisk symbols (*) indicate the altitudes of cloud bases observed with the mm-wave radar over the MU radar site. The straight line indicates the locus of the radiosonde launched at 1500 LT.

LT, when the most developed cirrus clouds with the thickness of >2 km were observed, the updraft was dominant at 8.5–12-km altitudes with the maximum (>0.75 m s^{-1}) at 9–10 km. It suggests that the cirrus clouds at least were developed up to the 10-km altitude due to the background updraft. After 1530 LT, the downdraft region extended from a 2- to 9.5-km altitude. The downdraft became >0.15 m s^{-1} almost at 2–9.5-km altitudes. It is coincident that the cirrus clouds decayed after 1530 LT.

Figure 9c shows time–altitude variations of vertical shear of the horizontal wind obtained with the MU radar. The layer with strong vertical shear existed at 8–9-km altitudes. The cloud-base altitude was generally located just above the altitude where the strong shear layer existed. The correspondence between cirrus cloud base and the layer of strong vertical shear of the horizontal wind was previously shown by Gultepe et al. (1995).

3) VERTICAL DOPPLER VELOCITY OBSERVED BY THE MM-WAVE RADAR

Figure 10 shows time–altitude variations of the vertical Doppler velocity observed with the mm-wave radar during 1400–1700 LT 6 October, and Fig. 11 shows the averaged profiles of the vertical velocity observed with the MU radar and vertical Doppler velocity observed with the mm-wave radar during 1430–1530 LT 6 October.

The reflectivity-weighted particle fall velocity relative to the ground increased when and where the large reflectivity was observed. For example, the reflectivity-weighted particle fall velocity increases >2.0 m s^{-1} when and where the reflectivity was larger than 12 dBZ (e.g. at 7.5–10 km during 1510–1530 LT). An updraft of 0.2–0.3 m s^{-1} was observed at 8.5–11-km altitudes. It suggests that the updraft at 8.5–11-km altitudes worked as one of the important factors for the development of cirrus clouds (see Fig. 9a). The reflectivity-weighted particle fall velocity was between 2.5 and 2.0 m s^{-1}. As we mentioned in section 3b(3), the reflectivity-weighted particle fall velocity was 1–2 m s^{-1}, and the reflectivity was generally <−16 dBZ in the cirrus clouds observed on 5 October (see Figs. 5a and 7). Therefore, our results show the increase of the reflectivity-weighted particle fall velocity in well-developed cirrus clouds. The reflectivity-weighted particle fall velocity was smaller (0.5–1.5 m s^{-1}) at the upper part of the cirrus clouds (10.5–11.5-km altitudes) than at the bottom part of the cirrus clouds (7.5–10.5-km altitudes). It shows that there were relatively small particles with small reflectivity-weighted particle fall velocities in the upper part of the cirrus clouds. Note that the sensitivity of the mm-wave radar was −24 dBZ at the 12-km altitude. Wang and Sassen (2001) showed that the mm-wave radar cannot observe a top portion of cirrus clouds, even with a sensitivity of −40 dBZ. Therefore, the mm-wave radar might fail to detect the cloud top, considering that the updraft region existed up to the 12-km altitude.

4) OBSERVATIONAL RESULTS WITH RADIOSONDE

Figure 12 shows altitude profiles of the humidity, potential temperature, and Brunt–Väisälä frequency ob-

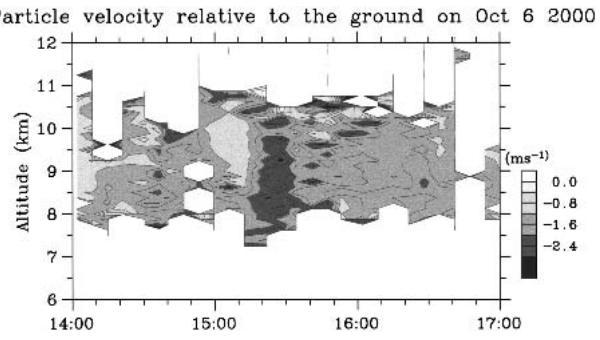

FIG. 10. Same as Fig. 6, but for 1400–1700 LT 6 Oct 2000.

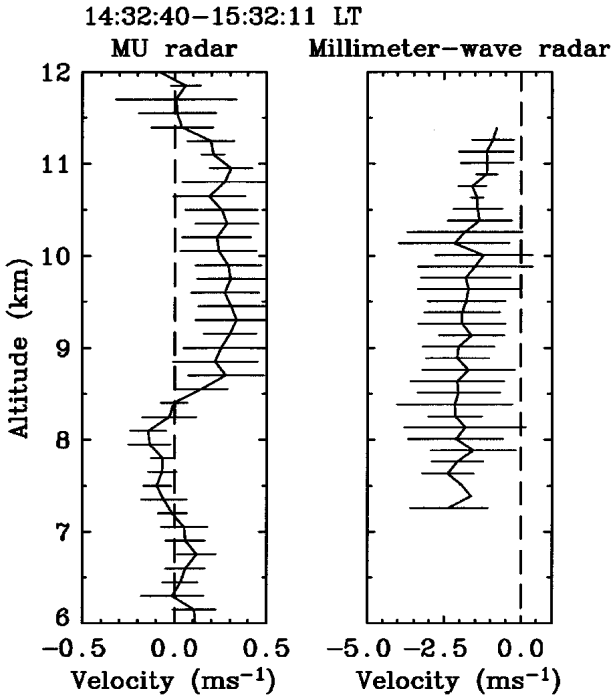

FIG. 11. Same as Fig. 7 but for 1430–1530 LT 6 Oct 2000.

served with the radiosonde launched at 1500 LT from the MU Observatory. The radiosonde reached the altitude of the cirrus clouds (8–10-km altitude) between 1535 and 1540 LT (see Fig. 9b). The vertical gradient of potential temperature was almost zero at approximately a 7.5-km altitude, at which the cirrus cloud base was located (see Fig. 8). This indicates that the cirrus cloud base was convectively unstable. Gultepe and Starr (1995) previously showed the similar result. The Brunt–Väisälä frequency was large ($>1.5 \times 10^{-3}$ rad^2 s^{-2}) at 7.8–8.5-km altitudes. It shows that the hydrostatic stability was large above the convectively unstable layer. At 1800 LT (0900 UTC) 6 October, the equivalent potential temperature derived from RANAL showed that the front with a low equivalent potential temperature (<320 K) existed below the 8.5-km altitude, and a high equivalent potential temperature (>330 K) existed above the 8.5-km altitude (not shown). Therefore, the equivalent potential temperature sharply increased with altitude around 7.8–8.5 km altitudes, and made the region hydrostatically stable. On the other hand, the Brunt–Väisälä frequency was small ($<0.1 \times 10^{-3}$ rad^2 s^{-2}) at 8.5–12.5-km altitudes.

5) CELL ECHOES

Figure 13 shows time variations of reflectivity obtained with the SRHI mode of the mm-wave radar from 240° in azimuth between 1527 and 1533 LT. At 1527 LT, there were strong cell echoes (>−8 dBZ) at a 20–24-km distance from the radar. These cell echoes moved with the background wind toward the mm-wave radar and became weaker at 1533 LT. The Richardson number shown in the right panel of Fig. 12 is calculated from the vertical shear of the horizontal wind obtained with the MU radar and the Brunt–Väisälä frequency obtained with the radiosonde. The Richardson number was <0.25 between 8.5- and 9.3-km altitudes around 1537–1539 LT. This result strongly suggests that KHI occurred between 8.5- and 9.3-km altitudes. It suggests that cell echoes were shaped by KHI (see Fig. 2 of Fritts and Rastogi 1985).

At 1800 LT (0900 UTC) 6 October, the equivalent potential temperature derived from RANAL showed that the atmosphere with low equivalent potential temperature (<320 K) and low relative humidity (<50%)

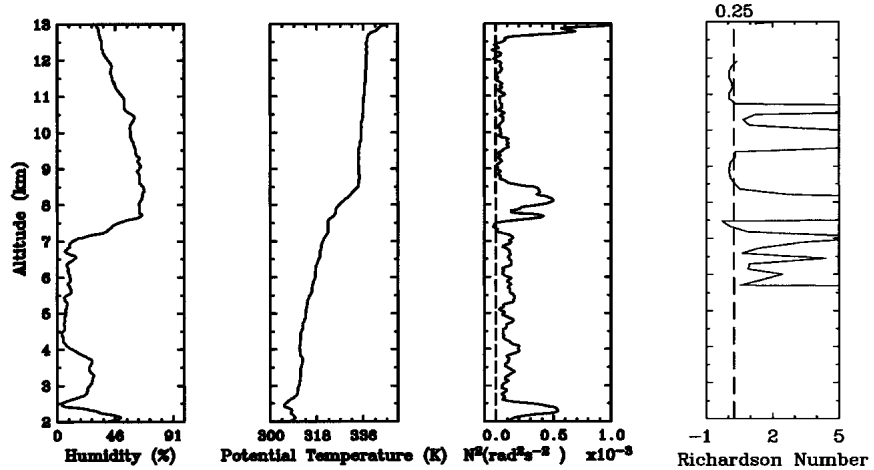

FIG. 12. Altitude profiles of humidity, potential temperature, Brunt–Väisälä frequency (N^2) and Richardson number obtained with a radiosonde launched at 1500 LT 6 Oct 2000. The Richardson number profile was calculated from vertical shear of the horizontal wind obtained with the MU radar.

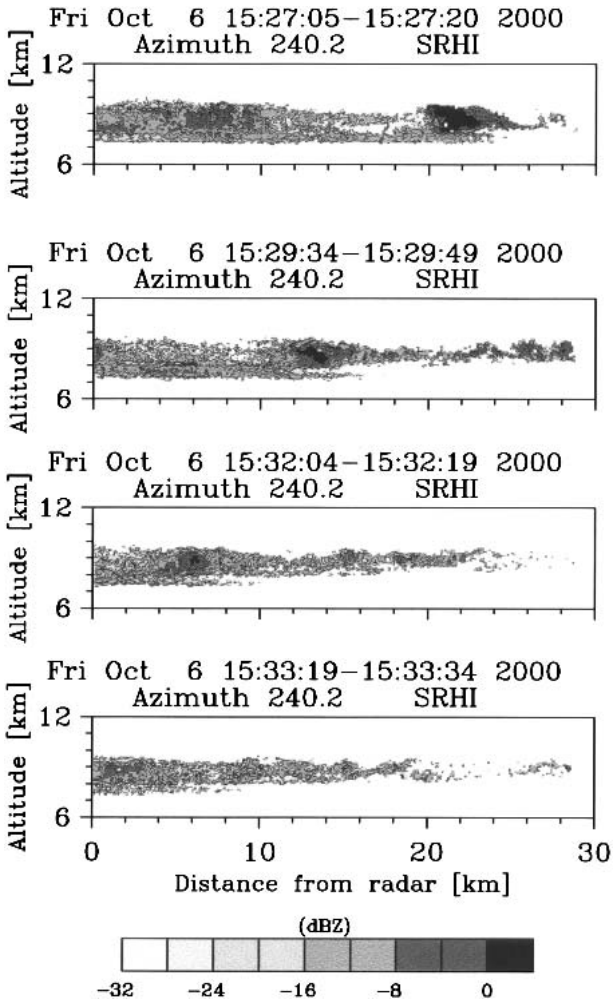

FIG. 13. RHI plots showing time variations of echo power observed with the mm-wave radar between 1527 and 1533 LT 6 Oct 2000.

existed below the 8.5-km altitude, and the atmosphere with high equivalent potential temperature (>330 K) and high relative humidity (>50%) existed above the 8.5-km altitude (not shown). The strong vertical shear of the horizontal wind that existed at 8–9-km altitudes generated KHI, and the KHI caused the airmass mixing above and below the 8.5-km altitude. The large echo power of >-4 dBZ existed at 8.5–9.5-km altitudes. This suggests that the cirrus clouds with large particles were formed by KHI. It is considered that large particles in the cirrus clouds existed at 8.5–9.5 km, because the mm-wave radar receives an echo from ice particles by Rayleigh scattering, and the reflectivity is proportional to the sixth power of the mean diameter of ice particles when ice particles of the same number exist at the same range.

On 6 October the thick cirrus clouds were developed at least up to a 10-km altitude during 1430–1530 LT (see Fig. 10). At the same time, the updraft of 0–0.3 m s^{-1} was observed at 8.5–12-km altitudes (see Fig. 11). This updraft contributed to the formation of thick cirrus clouds with a cloud top of at least 10 km, though the reflectivity-weighted particle fall velocity relative to the ground observed by the mm-wave radar was >1 m s^{-1} at 8.5–11-km altitudes (see Fig. 11). Considering that the size distribution of cirrus cloud particles can be well described by a gamma function (Matrosov et al. 1994), small ice particles that could not be detected by the mm-wave radar also existed at 8–9-km altitudes. Small ice particles could be transported upward by the updraft, because their reflectivity-weighted fall velocities relative to the air were smaller than the updraft. While they were transported upward, they were developed into large ice particles by aggregation, then formed the thick cirrus clouds with the thickness of >2 km.

4. Summary

We carried out the simultaneous observation of frontal cirrus clouds and background winds using the mm-wave radar and the MU radar during 30 September–13 October 2000. In this paper, we showed case studies on 5 and 6 October. Comparing observation results on 5 and 6 October, we showed that the development of cirrus clouds with large particles largely depended on the background vertical shear of the horizontal wind and the vertical wind. The frontal line on 6 October was located nearer to the MU Observatory than that on 5 October. Therefore, the vertical wind and the vertical shear of the horizontal wind were stronger and the shear layer was thicker in the case for 6 October than that for 5 October. The observed Richardson number (<0.25) strongly suggested that KHI occurred due to the strong vertical shear of the horizontal wind at 8–9-km altitudes on 6 October. The cell echoes of the cirrus clouds observed by the mm-wave radar also suggested that the airmass mixing by KHI caused the formation of cirrus clouds. The updraft of 0–0.3 m s^{-1} was observed by the MU radar at 8.5–12-km altitudes. The existence of the updraft in the region caused the development of thick cirrus clouds (>2 km) with large particles on 6 October.

We must mention that the sensitivity of the mm-wave radar is -16 (-27) dBZ at the 20 (10)-km range. Therefore, our observation may miss detection of the real cloud top due to lack of sensitivity to small particles in the cirrus clouds. However, in our case the sensitivity of the mm-wave radar is sufficient to discuss the growth of cirrus clouds with large particles, because the mm-wave radar successfully detected the growth of cirrus clouds with large particles. Note that it is very difficult for ground-based mm-wave radars to attain a sensitivity of better than -40 dBZ at a 10-km range because a very high power transmitter and a large antenna are necessary to attain this sensitivity. However, we believe that this work shows that a ground-based scanning mm-

wave radar is a useful tool for observing the three-dimensional structure of cirrus clouds simultaneously and continuously, and that KHI and updrafts in and around cirrus clouds play important roles on the generation of thick cirrus clouds with large particles. The quantitative relationship between KHI and the size of ice particle remains to be studied in subsequent studies. The existence and microphysical properties of cirrus clouds with small particles that we might fail to detect in the observation can be detected by a lidar. As future work, we are planning simultaneous observations by a mm-wave radar, lidar, radiosondes, and the MU radar. The quantitative relationships between the microphysical properties of cirrus clouds and background wind conditions will be clarified in subsequent studies.

Acknowledgments. We thank Dr. Gernot Hassenpflug and Dr. William L. Oliver Jr. for their careful reading of the manuscript. RANAL data were provided by the Japan Meteorological Agency. The MU radar belongs to and is operated by the Research Institute for Sustainable Humanosphere, Kyoto University. The present study was financially supported by Grants-in-Aids (12740270) of the Japanese Ministry of Education, Culture, Sports, Science, and Technology.

REFERENCES

Arnott, W. P., Y. Dong, R. Purcell, and J. Hallett, 1995: Direct airborne sampling of small ice crystals and the concentration and phase of haze particles. Preprints, *Ninth Symp. on Meteorological Observations and Instrumentation,* Charlotte, NC, Amer. Meteor. Soc., 415–420.

Braham, R. R., 1967: Cirrus cloud seeding as a trigger for storm development. *J. Atmos. Sci.,* **24,** 311–312.

Chepfer, H., G. Brogniez, L. Sauvage, P. H. Flaman, V. Trouillet, and J. Pelon, 1999: Remote sensing of cirrus radiative parameters during EUCREX'94. Case study of 17 April 1994. Part II: Microphysical models. *Mon. Wea. Rev.,* **127,** 504–519.

Fritts, D. C., and P. K. Rastogi, 1985: Convective and dynamical instabilities due to gravity wave motions in the lower and middle atmosphere: Theory and observations. *Radio Sci.,* **20,** 1247–1277.

Fukao, S., T. Sato, T. Tsuda, S. Kato, K. Wakasugi, and T. Makihira, 1985a: The MU radar with an active phased array system: 1. Antenna and power amplifiers. *Radio Sci.,* **20,** 1155–1168.

——, T. Tsuda, T. Sato, S. Kato, K. Wakasugi, and T. Makihira, 1985b: The MU radar with an active phased array system: 2. In-house equipment. *Radio Sci.,* **20,** 1169–1176.

Gayet, J. F., G. Febvre, and H. Larsen, 1996: The reliability of the PMS FSSP in the presence of small ice crystals. *J. Atmos. Oceanic Technol.,* **13,** 1300–1310.

Gultepe, I., and D. O'C. Starr, 1995: Dynamical structure and turbulence in cirrus clouds: Aircraft observations during FIRE. *J. Atmos. Sci.,* **52,** 4159–4182.

——, ——, A. J. Heymsfield, T. Uttal, T. Ackerman, and D. Westphal, 1995: Dynamical characteristics of cirrus clouds from aircraft and radar observations in micro and meso-γ scales. *J. Atmos. Sci.,* **52,** 4060–4078.

Hamazu, K., T. Wakayama, S. Watanabe, H. Hashiguchi, and S. Fukao, 2000: Development of a Ka-band Doppler radar for cloud and fog observations (in Japanese). *Trans. Inst. Electron. Inf. Commun. Eng.,* **J83-B,** 582–593.

——, ——, H. Hashiguchi, H. Tanaka, and S. Fukao, 2001: Preliminary field evaluation of a Ka-band Doppler radar for cloud and fog observation (in Japanese). *Trans. Inst. Electron. Inf. Comm. Eng.,* **J84-B,** 582–593.

——, H. Hashiguchi, T. Wakayama, T. Matsuda, R. J. Doviak, and S. Fukao, 2003: A 35-GHz scanning Doppler radar for fog observations. *J. Atmos. Oceanic Technol.,* **20,** 972–986.

Heymsfield, A. J., and G. M. McFarquhar, 1996: High albedos of cirrus in the tropical Pacific warm pool: Microphysical interpretation from CEPEX and from Kwajalein, Marshall Islands. *J. Atmos. Sci.,* **53,** 2424–2451.

Lynch, D., K. Sassen, D. O'C. Starr, and G. L. Stephens, Eds., 2002: *Cirrus.* Oxford University Press, 480 pp.

Matrosov, S. Y., B. W. Orr, R. A. Kropfli, and J. B. Snider, 1994: Retrieval of vertical profiles of cirrus cloud microphysical parameters from Doppler radar and infrared radiometer measurements. *J. Appl. Meteor.,* **33,** 617–626.

Muschinski, A., 1996: Possible effect of Kelvin-Helmholz instability on VHF radar observations of the mean vertical wind. *J. Appl. Meteor.,* **35,** 2210–2217.

Sato, T., H. Doji, H. Iwai, I. Kimura, S. Fukao, M. Yamamoto, T. Tsuda, and S. Kato, 1990: Computer processing for deriving drop-size distributions and vertical air velocities from VHF Doppler radar spectra. *Radio Sci.,* **25,** 961–973.

Sauvage, L., H. Chepfer, V. Trouillet, P. H. Flamant, G. Brogniez, J. Pelon, and F. Albers, 1999: Remote sensing of cirrus radiative parameters during EUCREX'94. Case study of 17 April 1994. Part I: Observations. *Mon. Wea. Rev.,* **127,** 486–503.

Stephens, G. L., 1995: Editorial: First ISCCP Regional Experiment Intensive Field Observations II. *J. Atmos. Sci.,* **52,** 4041.

Stokes, G. M., and S. E. Schwartz, 1994: The Atmospheric Radiation Measurement (ARM) Program: Programmatic background and design of the cloud and radiation testbed. *Bull. Amer. Meteor. Soc.,* **75,** 1201–1221.

Uchiyama, A., and M. Fukabori, 1999: Ground-based cirrus observation: II. Spectral properties of cirrostratus clouds in the 8–12 μm. *J. Meteor. Soc. Japan,* **77,** 533–552.

——, S. Asano, M. Shiobara, and M. Fukabori, 1999: Ground-based cirrus observation: I. Observation system and results of frontal clouds. *J. Meteor. Soc. Japan,* **77,** 513–532.

Wakasugi, K., A. Mizutani, M. Matsuo, S. Fukao, and S. Kato, 1986: A direct method for deriving drop-size distribution and vertical air velocities from VHF Doppler radar spectra. *J. Atmos. Oceanic Technol.,* **3,** 623–629.

Wang, Z., and K. Sassen, 2001: Cloud type and property retrieval using multiple remote sensors. *J. Appl. Meteor.,* **40,** 1665–1682.

Yamamoto, M., T. Sato, P. T. May, T. Tsuda, S. Fukao, and S. Kato, 1988: Estimation error of spectral parameters of mesosphere–stratosphere–troposphere radars obtained by least squares fitting method and its lower bound. *Radio Sci.,* **23,** 1013–1021.